A high-temperature approximation for the path-integral quantum Monte Carlo method

1996 J. Phys. A: Math. Gen. 29 3471

(http://iopscience.iop.org/0305-4470/29/13/018)

J. Phys. A: Math. Gen. **29** (1996) 3471–3494. Printed in the UK

A high-temperature approximation for the path-integral quantum Monte Carlo method

M Kolář† and S F O'Shea

Department of Chemistry, University of Lethbridge, Lethbridge, Alberta, Canada T1K 3M4

Received 18 August 1995, in final form 6 February 1996

Abstract. A high-temperature approximation for the discretized path-integral quantum Monte Carlo (PIQMC) method is formulated. At higher temperatures, all P fictitious classical particles representing a single quantum particle stay close together, and an efficient approximation is obtained when, in the primitive short-time propagator, an essentially local harmonic approximation is used for the external potential at the common centre of mass of P fictitious particles—the integration over $P-1$ dimensions can then be carried out analytically, and a classical formula of the effective-potential type is obtained for the partition function.

Also discussed are the proper form and applicability of the virial total-energy estimator for finite systems, and the computation of the temperature dependence of the configurational partition function in a single PIQMC run.

1. Introduction

The success of the classical NVT ensemble (Metropolis) Monte Carlo (MC) method [1] led to a considerable interest in devising the quantum variants of the method based on the Feynman's path integral formulation of the density matrix [2, 3]. For bosons, two versions of the path-integral quantum Monte Carlo (PIQMC) method have been formulated—the discretized PIQMC method [4–8], and the Fourier PIQMC method [9, 10]. Various real systems have already been successfully studied using these methods [8, 11]. Nevertheless, it remains important to look for ways to speed up their convergence. One way to achieve this goal is to construct more accurate short-time propagators [12–16]. A complementary approach is to use the Gibbs inequality to 'average away' at least some of the P isomorphic degrees of freedom. The simplest approximation of this kind is the Feynman–Hibbs effective potential method [2, 3]. A similar Gaussian transform of the potential is used in the partial averaging of the Fourier PIQMC method [10], which can be arbitrarily refined. Another, more complicated approach is to combine the use of the Gibbs inequality with perturbational and variational procedures [17].

Here we proceed along yet another path. The initial impulse for this work came from our exploration of the use of PIQMC simulations for the study of surface adsorption. It led us to the formulation of an approximate discretized PIQMC method that is as simple as the Feynman–Hibbs effective potential method. However, our 'effective potential' does not involve a Gaussian transform at all. Here we stay within the confines of the primitive (constant-potential) short-time propagator within the discretized PIQMC method. In the

† Present address: AECL Research, Whiteshell Laboratories, Pinawa, Manitoba, Canada R0E 1L0; e-mail: kolarm@wl.aecl.ca

0305-4470/96/133471+24$19.50

coordinate system corresponding to normal modes of the isomorphic polymer, we expand the external potential about the common centre of mass of the P fictitious classical particles, truncate the potential at the quadratic term at the most, and use this truncated potential in the primitive short-time propagator. The end product is an approximate formula for the quantum partition function that can be written in the form of a classical formula with quantum corrections. In the $P \to \infty$ limit this approximation gives exact results at high temperatures in all cases, and for the harmonic oscillator potential this applies *at all temperatures*, and it is expected to give good results in a wide temperature range for a class of anharmonic oscillator potentials. Even at low temperatures this approximation seems to be much better than previous approximations of comparable complexity [3, 10] that do not give exact results even for the harmonic oscillator potential.

In section 2 the discretized PIQMC method is reviewed briefly and the proper form of the virial total-energy estimator for box-like potentials established. PIQMC simulations for the 9–3 potential of appendix A and the usefulness of the corrected virial estimator for this potential are discussed in section 3. In section 4 the direct quasi-random integration of the P-dimensional integrals for the ensemble averages occurring in the PIQMC method is described. The insight obtained in sections 3 and 4 is then used in the formulation of the approximate high-temperature PIQMC method in section 5. Some technical details are presented in the appendices. In section 6 the possibility of obtaining the temperature dependence of a configurational partition function in a single PIQMC run is demonstrated.

2. The discretized PIQMC method and the virial total-energy estimator

In the discretized PIQMC method based on the primitive short-time propagator [4–8], the quantum canonical partition function of one particle in the external potential $V(x)$ is approximated by that of a cyclic chain of P classical particles, which, in one dimension, is

$$Q_P = C^{P/2} \int \mathrm{d}x_1 \cdots \int \mathrm{d}x_P \, \mathrm{e}^{-\beta U_P} \tag{1}$$

where

$$U_P = \alpha_P + \lambda_P \qquad \alpha_P = \frac{C\pi}{\beta} \sum_{t=1}^{P} (x_t - x_{t+1})^2 \qquad \lambda_P = \frac{1}{P} \sum_{t=1}^{P} V(x_t) \tag{2}$$

$C = mP/2\pi\beta\hbar^2$, $x_{P+1} \equiv x_1 \equiv x$, and $\beta = 1/kT$ is the reciprocal temperature. Equation (1) can be written as

$$Q_P = \int \mathrm{d}x_1 \, \rho_P(x_1, x_1, \beta)$$

where ρ_P is the P-approximation of the canonical density matrix, whose diagonal matrix elements are

$$\rho_P(x, x, \beta) \equiv \rho_P(x) = C^{P/2} \int \mathrm{d}x_2 \cdots \int \mathrm{d}x_P \, \mathrm{e}^{-\beta U_P}. \tag{3}$$

Substituting Q_P in the total-energy formula

$$\langle E \rangle = -\frac{\partial \ln Q}{\partial \beta} \tag{4}$$

yields the approximation

$$\epsilon_P = \frac{P}{2\beta} - \alpha_P + \lambda_P. \tag{5}$$

Herman *et al* [6] have shown that the variance $\langle \delta\epsilon_P^2 \rangle = \langle (\epsilon_P - \langle \epsilon_P \rangle)^2 \rangle$ of this estimator diverges as $P \to \infty$. They have also shown that in an infinite Hilbert space a virial theorem applies, and another good total-energy estimator is the virial estimator,

$$\epsilon_P^{\mathrm{vir}} = \frac{1}{2P} \sum_{t=1}^{P} x_t \frac{\partial V(x_t)}{\partial x_t} + \lambda_P \tag{6}$$

which has finite variance as $P \to \infty$.

For a potential defined only in the finite interval $(x_{\min}, x_{\max})$, the limits of integration in all integrals in equations (1) and (3) are $x_{\min}$ and $x_{\max}$. In this case, the average value $\langle \epsilon_P^{\mathrm{vir}} \rangle$ of the virial estimator of equation (6) depends on the origin of coordinates,

$$\langle \epsilon_P^{\mathrm{vir}} \rangle = \langle \epsilon_P \rangle - \frac{P}{2\beta Q_P} \phi \tag{7}$$

where

$$\begin{aligned} \phi &= x_{\max} \rho_P(x_{\max}) - x_{\min} \rho_P(x_{\min}) \\ &= x_{\min} [\rho_P(x_{\max}) - \rho_P(x_{\min})] + L \rho_P(x_{\max}) \end{aligned} \tag{8}$$

$L = x_{\max} - x_{\min}$, and Q_P and ρ_P are given by equations (1) and (3). By equation (7), $\epsilon_P^{\mathrm{vir}}$ is not always a good total-energy estimator. Whereas the exact densities must be equal to zero at the system boundaries, $\rho(x_{\min}) = \rho(x_{\max}) = 0$, this is not true for their P-approximants ρ_P. For example, in a symmetric system when $\rho_P(x_{\max}) = \rho_P(x_{\min}) \neq 0$, $\langle \epsilon_P^{\mathrm{vir}} \rangle$ is consistently less positive or more negative than $\langle E \rangle \equiv \langle \epsilon_P \rangle$.

If $\rho_P(x_{\max}) \neq \rho_P(x_{\min})$, ϕ depends on the position of the coordinate origin and can always be made equal to zero by the following coordinate transformation: $x' = x + x_0 - x_{\min}$, where

$$x_0 = -\frac{L \rho_P(x_{\max})}{\rho_P(x_{\max}) - \rho_P(x_{\min})}. \tag{9}$$

In the new coordinate system $x'_{\min} = x_0$, and equation (8) gives $\phi' = 0$. The virial estimator corresponding to this special choice of coordinate origin, expressed in the old coordinate system, is

$$\epsilon_P^{\mathrm{vir0}} = \frac{1}{2P} \sum_{t=1}^{P} (x_t + x_0 - x_{\min}) \frac{\partial V(x_t)}{\partial x_t} + \lambda_P. \tag{10}$$

Then

$$\langle \epsilon_P^{\mathrm{vir0}} \rangle = \langle \epsilon_P \rangle.$$

In a general case, the disadvantage of $\epsilon_P^{\mathrm{vir0}}$ is that one has to know in advance $\rho_P(x_{\min})$ and $\rho_P(x_{\max})$ to be able to calculate x_0. However, if $V(x_{\min +}) = \infty$, $\rho_P(x_{\min}) = 0$ (see equation (3)) and $x_0 = -L$. This happens to be the case for the 9–3 potential of equations (A1) or (A3). For this potential $x_{\min} = 0$, and

$$\epsilon_P^{\mathrm{vir0}} = \frac{1}{2P} \sum_{t=1}^{P} (x_t - L) \frac{\partial V(x_t)}{\partial x_t} + \lambda_P. \tag{11}$$

Similarly, if $V(x_{\max -}) = \infty$, $\rho_P(x_{\max}) = 0$ and $x_0 = 0$.

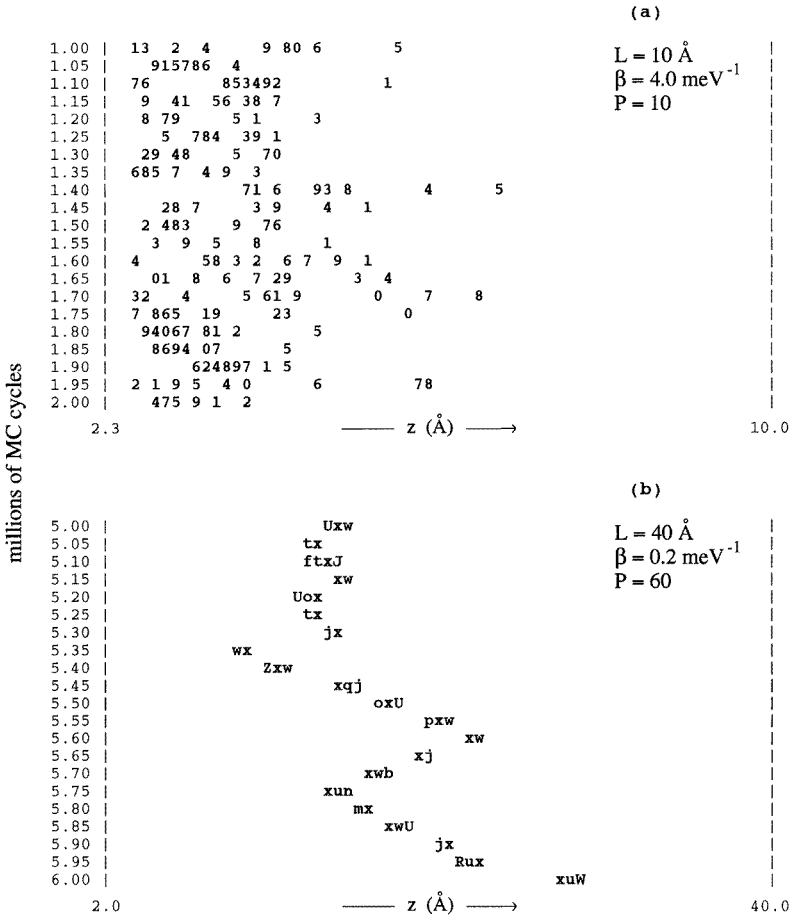

Figure 1. Localization of the quantum particle as a function of inverse temperature. In this schematic representation of the isomorphic polymer, particles 1 to P are represented consecutively by the first P symbols from the series 0, 1, 2,..., 9, A, B,..., Z, a, b,..., z. The polymer may be folded over itself many times, with more than one polymer particle in a given bin in the histogram of z, the height above the surface; only the highest index is shown in each bin. Data for parts of two different runs, without the whole-polymer moves, are shown every 50 000 MC cycles for the truncated 9–3 potential with $z_0 = 3$ Å, $V_m = 4.8$ meV, $m = 1837.151\,52 m_{\mathrm{el}}$.

3. Path-integral quantum Monte Carlo simulations for the 9–3 potential

In this section, we briefly review the results of the standard discretized PIQMC simulations for the truncated 9–3 potential of appendix A, with parameters corresponding to H of a molecule of HF adsorbed on the surface of solid LiF [18] ($m = 1837.152 m_{\mathrm{el}}$, $z_0 = 3$ Å, $V_m = 4.8$ meV). For these values, the ground-state energy is $E_0 = -1.9020$ meV.

At low temperatures ($\beta \gtrsim 2$ meV^{-1}) the particle shows strong quantum behaviour, being well delocalized (figure 1(a)), and good convergence is obtained using the simple PIQMC method. For high temperatures ($\beta \lesssim 1$ meV^{-1}) and large L, whole-polymer moves must be attempted periodically to speed up the sampling of the whole allowed z range (cf

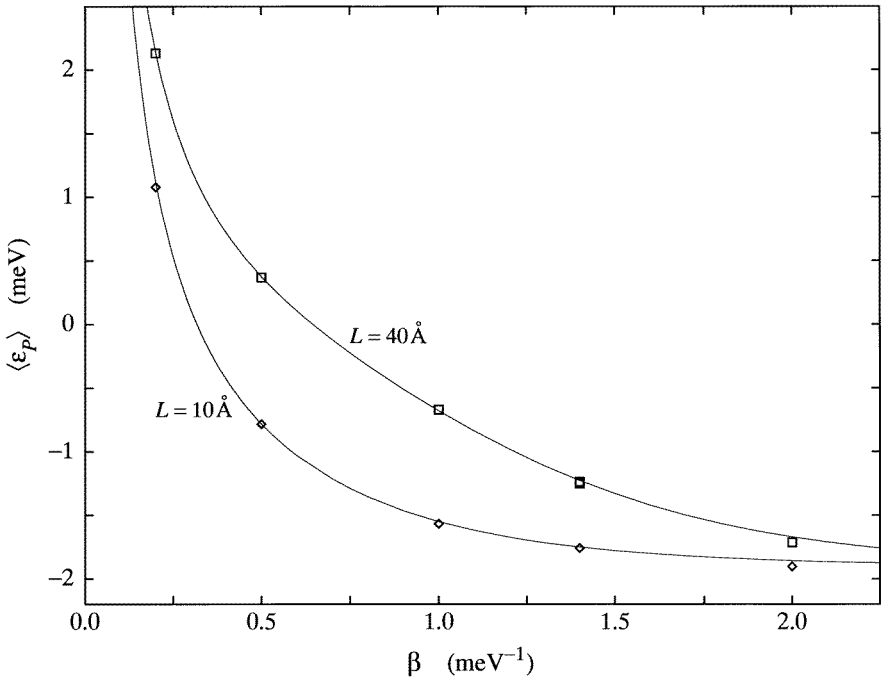

Figure 2. The converged path-integral quantum Monte Carlo results for $\langle\epsilon_P\rangle$ for the same 9–3 potential as in figure 1. Diamonds (◊): $L = 10$ Å {$\beta \geqslant 1.4$ meV^{-1}: 10^7 cycles, $P = 60$; $\beta = 1.0$ meV^{-1}: 10^7 cycles, $P = 40$; $\beta = 0.5$ meV^{-1}: 4×10^7 cycles, $P = 40$; $\beta = 0.2$ meV^{-1}: 2.5×10^7 cycles, $P = 10$}. Boxes (□): $L = 40$ Å {$\beta = 1.0$ and 2.0 meV^{-1}: 10^7 cycles, $P = 60$; $\beta = 1.4$ meV^{-1}: 1.5×10^7 cycles, $P = 60$, four different values of the maximum whole-polymer shift (2–10 Å) used; $\beta = 0.5$ meV^{-1}: 2.6×10^7 cycles, $P = 40$; $\beta = 0.2$ meV^{-1}: 4×10^7 cycles, $P = 10$}. In all cases except for $L = 10$ Å and $\beta \geqslant 1.4$ meV^{-1}, whole-polymer moves were performed. Full curves labelled by L represent the exact values of $\langle E\rangle$ of equation (A4).

figure 1(b)) where without the whole-polymer moves only a small part of the allowed range was sampled in 10^6 cycles). Figure 2 shows that by using large enough values of P for different values of β and L excellent agreement of the PIQMC results with the exact values of $\langle E\rangle$ can be obtained. For $\beta = 2.0$ meV^{-1}, $P = 60$ is clearly still not large enough. The dependence of the converged $\langle\epsilon_P\rangle$ on P is illustrated in figure 3.

Figure 4 compares the exact (as obtained by the diagonalization procedure mentioned in appendix A) quantum-mechanical particle density $(1/Q)\rho(z, z, \beta)$ with the average density of quantum polymer particles for one of the simulations of figure 2. The discrepancy at the density peak is an artifact of the averaging occurring in a histogram bin of width Δz used to evaluate the PIQMC density.

As illustrated in figure 5, in accordance with equation (7), $\langle\epsilon_P^{\rm vir}\rangle$ is consistently less than $\langle\epsilon_P\rangle$; this difference decreases with β. Using $\langle\epsilon_P^{\rm vir0}\rangle$ to correct for the origin dependence, equation (11), produces close agreement with $\langle\epsilon_P\rangle$. The dependence of the variances of ϵ_P and $\epsilon_P^{\rm vir}$ on P, figure 6, is similar to that in the harmonic oscillator (cf figure 2 of [6]).

It seems that the corrected virial estimator $\epsilon_P^{\rm vir0}$ of equation (11) is not much more useful than $\epsilon_P^{\rm vir}$. Although the value of $\langle\epsilon_P^{\rm vir0}\rangle$ is close to $\langle\epsilon_P\rangle$ it is evident from figure 5 that its convergence to the same limit as $\langle\epsilon_P\rangle$ is extremely slow. In other cases, the rate

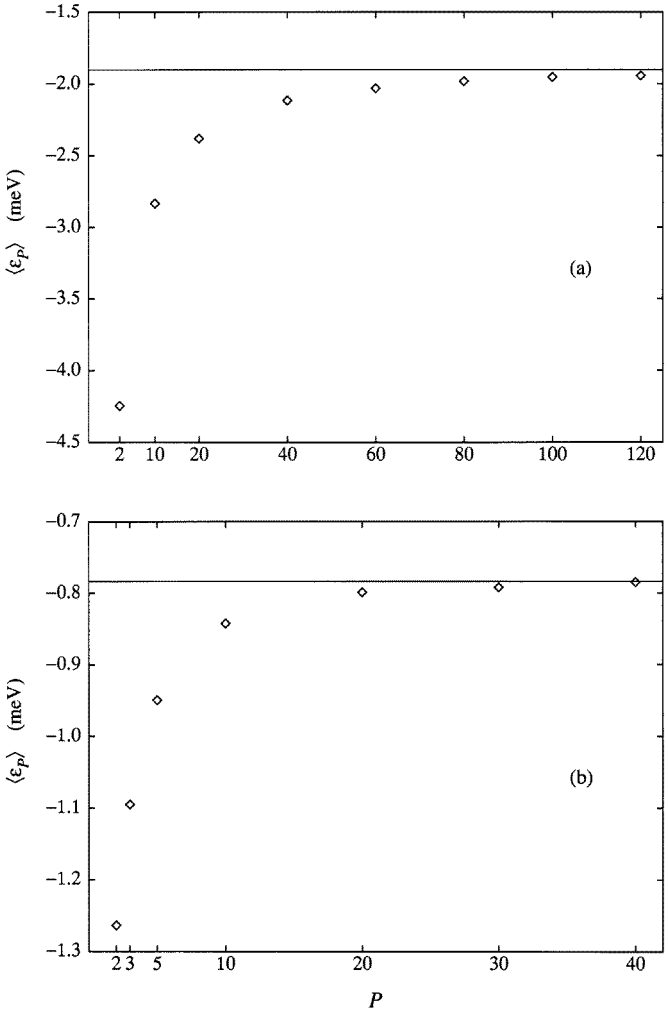

Figure 3. Dependence of $\langle \epsilon_P \rangle$ ($\Diamond$) on P. (a) $L = 10$ Å, $\beta = 4.0$ meV^{-1}, 2×10^6 cycles, no whole-polymer moves; (b) $L = 10$ Å, $\beta = 0.5$ meV^{-1}, 4×10^7 cycles, whole-polymer moves done every five cycles. Same potential as in figure 1. Full horizontal lines represent the exact values of $\langle E \rangle$ of equation (A4).

of convergence may be even more discouraging than that in figure 5: $\langle \epsilon_P^{\mathrm{vir0}} \rangle$ may fluctuate around $\langle \epsilon_P \rangle$ without any sign of damping, and its variance seems to always be much larger than that of $\epsilon_P^{\mathrm{vir}}$. For example, the values of $\langle \delta(\epsilon_P^{\mathrm{vir0}})^2 \rangle$ for 10^7 cycles corresponding to figure 6 ($\beta = 4.0$ meV^{-1}) vary from 42.65 meV^2 for $P = 2$ to 31.15 meV^2 for $P = 150$. It seems that $\langle \delta(\epsilon_P^{\mathrm{vir0}})^2 \rangle$ is always much larger than $\langle \delta(\epsilon_P^{\mathrm{vir}})^2 \rangle$ and $\langle \delta \epsilon_P^2 \rangle$ in the range of values of P required to get a satisfactory agreement of $\langle \epsilon_P \rangle$ with $\langle E \rangle$.

The fluctuations of $\epsilon_P^{\mathrm{vir0}}$ are evidently due to the presence of the $-L$ term in equation (11). Because of this term, the main contribution to $\langle \epsilon_P^{\mathrm{vir0}} \rangle$ comes from the region to the left of the minimum of the potential where the derivative of the potential is large and the sampling may not be satisfactory.

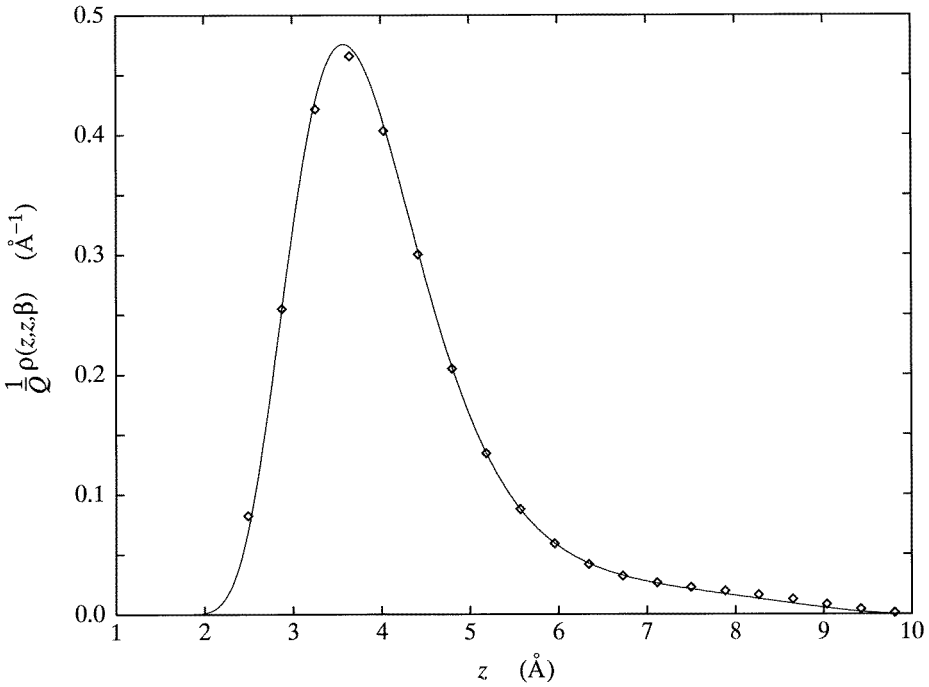

Figure 4. Comparison of the exact normalized particle density (full curve) with the PIQMC results (◇) for one simulation of figure 2: $L = 10$ Å, $\beta = 1.4$ meV^{-1}.

4. Direct integration of thermal averages for small β

In this section we prepare ground for the approximate PIQMC method formulated in the next section by exploring what contributes most to the PIQMC ensemble averages that are given by ratios of P-dimensional integrals of the type

$$\langle A_P \rangle = \frac{\int_{x_{\min}}^{x_{\max}} \mathrm{d}x_1 \cdots \int_{x_{\min}}^{x_{\max}} \mathrm{d}x_P \, A_P(x_1, \ldots, x_P) \mathrm{e}^{-\beta U_P}}{\int_{x_{\min}}^{x_{\max}} \mathrm{d}x_1 \cdots \int_{x_{\min}}^{x_{\max}} \mathrm{d}x \, P \mathrm{e}^{-\beta U_P}} \tag{12}$$

where $A_P(x_1, \ldots, x_P)$ are suitable estimators, for example those given by equations (5) or (11).

It can be seen from equation (2) that as $\beta \to 0$ ($T \to \infty$), α_P becomes extremely large except when all x_t are almost identical, i.e. near a body diagonal of the integration volume in equation (12)—a P-dimensional cube of edge $L = x_{\max} - x_{\min}$. P-dimensional integrals with the values of P used in the previous section for small β can be calculated using pseudo- or quasi-random grids (see e.g. [19, 20]). To speed up convergence, integration in equation (12) can be confined to a narrow 'channel' around the body diagonal where $\mathrm{e}^{-\beta U_P}$ is significantly different from zero. To make things simpler, a channel of rectangular cross section is chosen. A Cartesian coordinate system is used where one basis vector, $\boldsymbol{u}_1$, is parallel to the body diagonal, and all the others, $\boldsymbol{u}_2, \ldots, \boldsymbol{u}_P$, are perpendicular to it. The width of the integration channel is the same in all the directions $\boldsymbol{u}_2, \ldots, \boldsymbol{u}_P$, and will be denoted as Δ. One way to choose the components $\boldsymbol{u}_{ji}$ of the normalized vectors $\boldsymbol{u}_j$ is

$$u_{1i} = 1/\sqrt{P} \qquad i = 1, \ldots, P \tag{13}$$

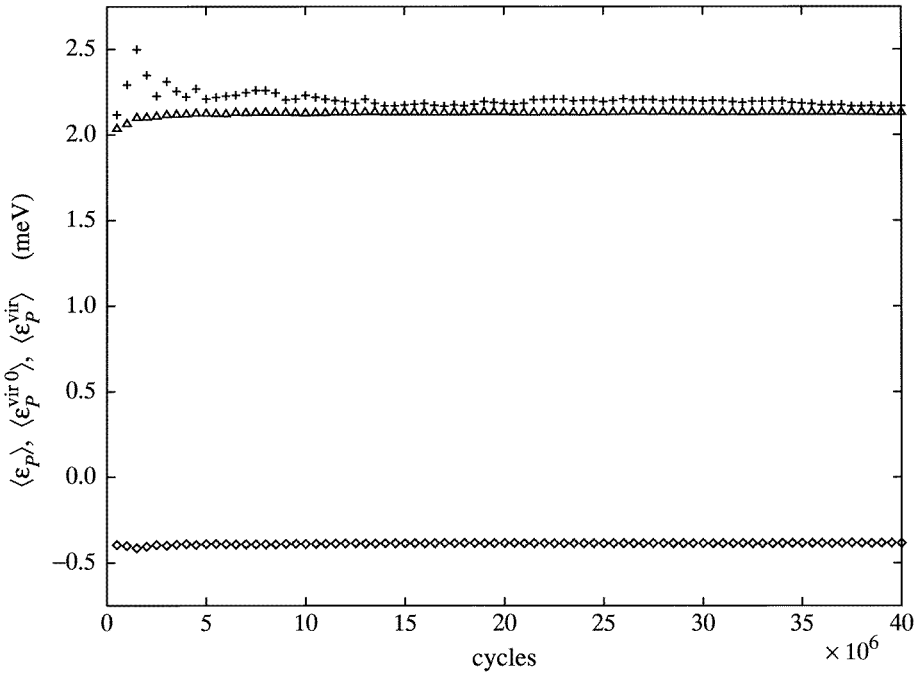

Figure 5. Comparison of the dependence on the number of cycles of $\langle\epsilon_P^{\mathrm{vir}0}\rangle(+)$ and $\langle\epsilon_P^{\mathrm{vir}}\rangle(\Diamond)$ with that of $\langle\epsilon_P\rangle(\triangle)$ for the ($\beta = 0.2$ meV^{-1}, $L = 40$ Å) point of figure 2.

and for $j > 1$,

$$u_{ji} = \begin{cases} 1/\sqrt{j(j-1)} & i < j \\ -\sqrt{(j-1)/j} & i = j \\ 0 & i > j \end{cases}$$

(another possible choice is discussed in the next section). The transformation to the new coordinates ξ_j thus reads

$$x_i = \sum_{j=1}^{P} \xi_j u_{ji}. \tag{14}$$

The reduced integration volume is the intersection of the P-dimensional rectangular prism determined by the inequalities

$$\frac{x_{\min}}{\sqrt{P}} \leqslant \xi_1 \leqslant \frac{x_{\max}}{\sqrt{P}} \qquad -\frac{\Delta}{2} \leqslant \xi_j \leqslant \frac{\Delta}{2} \qquad j \geqslant 2 \tag{15}$$

and the original cube

$$x_{\min} \leqslant x_i \leqslant x_{\max}. \tag{16}$$

Monte Carlo integration was performed as follows. A 'random' uniformly distributed P-dimensional point $(\eta_1, \ldots, \eta_P)$ in a unit cube, $0 \leqslant \eta_j < 1$, was generated using either the fast Halton quasi-random number generator [20] or the pseudo-random RANMAR generator [21]. This point was then mapped onto the prism (15) as follows:

$$\xi_1 = \frac{x_{\min} + \eta_1 L}{\sqrt{P}} \qquad \xi_j = (-\tfrac{1}{2} + \eta_j)\Delta \qquad j \geqslant 2.$$

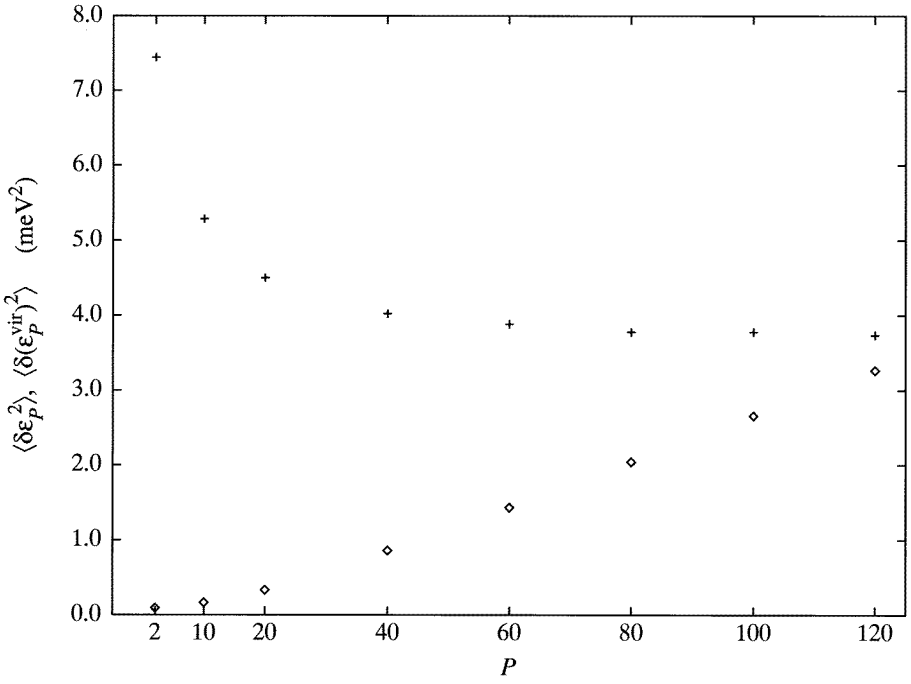

Figure 6. Dependence of $\langle \delta\epsilon_P^2 \rangle (\diamond)$ and $\langle \delta(\epsilon_P^{\rm vir})^2 \rangle (+)$ on P. Same parameters as in figure 3(a).

Then x_i were calculated using equation (14), and it was checked whether this point lies in the cube (16). If the answer was affirmative, integrands of all the integrals in question (several $\langle A_P \rangle$ can be calculated simultaneously) were calculated and added to the respective accumulators. One of the accumulators was set up for $e^{-\beta U_P}$ (the denominator in equation (12)). The total number of random points sampled in this way will be denoted as N in what follows.

The particle density $\rho_P(x)$, as given by equation (3), can be calculated in a similar way. For simplicity, for a given $x = x_1$, we integrate over a $(P-1)$-dimensional cube of edge Δ centred around the point where all coordinates are equal to x:

$$x - \frac{\Delta}{2} \leqslant x_i \leqslant x + \frac{\Delta}{2} \qquad i = 2, \ldots, P. \tag{17}$$

If this small cube 'sticks out' of the big cube of equation (16), we shift its centre along the diagonal of the big cube so that it is fully contained inside the big cube.

All the numerical results in this section were obtained using the Halton numbers with randomly selected starting points for individual vector components as described in [20], which were found to be as good for this purpose as the pseudo-random numbers generated by RANMAR, and might even lead to a somewhat faster convergence.

The value of Δ and the number N of the random grid points can be adjusted to give the best results. When Δ is too small, the integral already converges for small N, but the estimate of Q_P thus obtained is too small because $e^{-\beta U_P}$ is still large outside the prism (15). When Δ is too large, the generated quasi-random grid is so sparse that few points lie in the region near the main diagonal where $e^{-\beta U_P}$ is non-zero even for very large N, and the estimate of Q_P will again be too small. Let us denote by $Q_P(\Delta, N)$ the approximation to Q_P of equation (1) obtained with N quasi-random points uniformly distributed in the

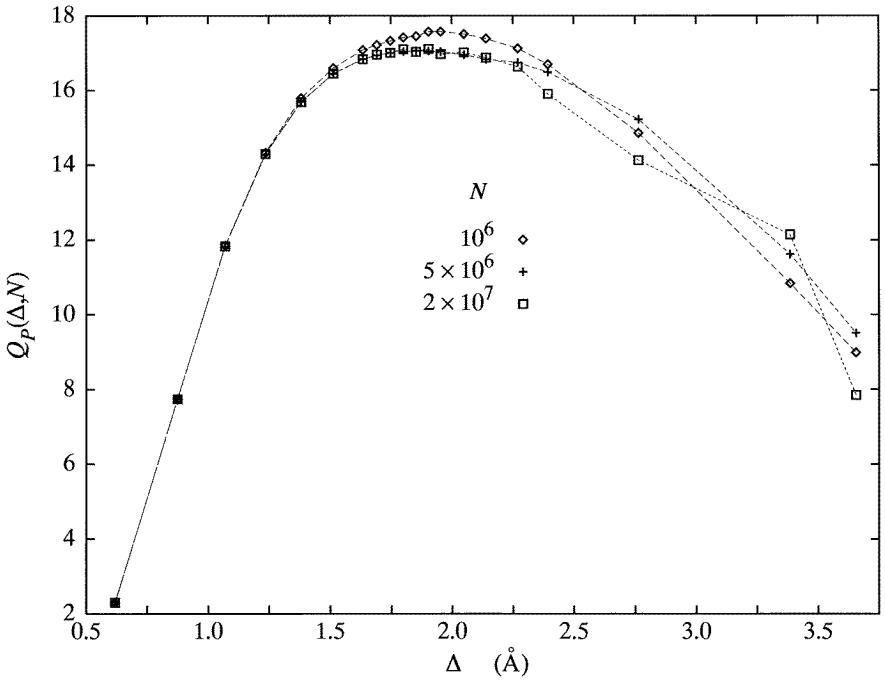

Figure 7. Dependence of $Q_P(\Delta, N)$ on Δ for several values of N; $P = 10$, $\beta = 0.2$ meV^{-1}. Same potential as in figure 1, $L = 40$ Å.

prism (15). Then $Q_P(\Delta, \infty)$ is expected to be a monotone function of Δ that at first increases rapidly and then, for $\Delta \gtrsim \Delta_0$, approaches a constant, equal to the exact value $Q_P = Q_P(\infty, \infty)$. Δ_0 corresponds to the situation when the prism (15) just circumscribes the region with non-zero $e^{-\beta U_P}$. To get the value of $Q_P(\Delta, \infty)$ for larger values of Δ requires extremely large N. Thus the best approach may be to plot $Q_P(\Delta, N)$ for a fixed N as a function of Δ. This function should have a maximum at $\Delta \approx \Delta_0$. When this maximum does not change any more as N is further increased (see figure 7), we can stop the integration and consider the values of various averages (12), obtained with the value of Δ corresponding to the position of the maximum of the $Q_P(\Delta, N)$ curve, as reasonable estimates that can be obtained in the shortest possible time.

Similarly, let us denote by $\rho_P(x; \Delta, N)$ an estimate to $\rho_P(x)$ obtained using N random $(P-1)$-dimensional points uniformly distributed in the cube (17). Again, for the same reason, $\rho_P(x; \Delta, N)$ with constant N has a maximum at certain Δ_0'. When this maximum does not change any more as N is further increased, we take it as a good approximation of $\rho_P(x)$. For $x = x_{\max}$, this estimate of $\rho_P(x)$ is usually much better than the one obtained from the PIQMC simulations as described in the previous section. The calculation of $\rho_P(x)$ seems to require larger values of N than that of Q_P and average energy.

For the parameters of figure 7 ($\beta = 0.2$ meV^{-1}) we have the following estimates: $Q_{10} = 17.1$, $\langle \epsilon_{10} \rangle = 2.1 \pm 0.05$ meV (the error estimate corresponds to the amplitude of the fluctuations of $\langle \epsilon_{10} \rangle$ between $N = 10^7$ and 2×10^7), $\langle \epsilon_{10}^{\rm vir} \rangle = -0.37$ meV (using the incorrect formula (6)), $\langle \epsilon_{10}^{\rm vir0} \rangle = 2.4$ meV. From a different MC integration for $\rho_{10}(x_{\max}; \Delta, N)$, we have $\rho_{10}(x_{\max}) = 0.0442$ Å^{-1}. These values give $(P/2\beta Q_P)\phi = 2.58$ meV, and thus equation (7) is very well satisfied with the error between its right- and left-hand sides

being of the order of 0.1 meV (recall that $\rho_P(x_{\min}) = 0$). For comparison, a PIQMC simulation gave $\langle \epsilon_{10} \rangle = 2.13$ meV (cf figure 2) and $\langle \epsilon_{10}^{\text{vir0}} \rangle = 2.17$ meV. The exact value is $\langle E \rangle = 2.143$ meV. Of course, the exact quantum density at $x_{\max}$ is always equal to zero. In this respect, the PIQMC method is always incorrect for finite P.

We have also performed modified calculations in which the integration was extended over the whole volume of the prism (15), i.e. the condition (16) was ignored. This only affected the results slightly, because for small β only a negligible portion of the prism (15) lies outside the big cube. Thus extending the integration limits to infinity everywhere in the direction perpendicular to the main diagonal $\boldsymbol{u}_1$ does not significantly change the results.

The CPU time required to obtain converged integrals of equation (12) for a single value of Δ is about half of the time needed for a corresponding PIQMC simulation with the same P. However, the total CPU time can be much larger due to the necessity of repeating the calculations for different values of Δ. We do not expect that this approach in its pure form will find any practical application. Perhaps it could find some use as part of a hybrid method along some directions of the configuration space in combination with the standard PIQMC simulation for the remaining degrees of freedom. An approximate approach along this line is formulated in the next section. The primary purpose of this section was to provide a starting point and some justification for the high-temperature approximation presented in section 5.

5. A high-temperature approximation for the PIQMC method

In this section, working in the normal-mode coordinates for α_P, we apply an essentially local harmonic approximation for all the occurrences of the external potential in equation (12). Most of the integrals occurring in equation (12) can then be evaluated analytically and an efficient high-temperature approximation of the PIQMC method (HTPIQMC) is obtained.

The formula for α_P of equation (2) can be written as

$$\alpha_P = \frac{C\pi}{\beta} \sum_{i,j=1}^{P} x_i (a_P)_{ij} x_j \tag{18}$$

where

$$a_2 = \begin{pmatrix} 2 & -2 \\ -2 & 2 \end{pmatrix} \tag{19a}$$

$$a_P = \begin{pmatrix} 2 & -1 & 0 & \cdots & 0 & -1 \\ -1 & 2 & -1 & \cdots & 0 & 0 \\ 0 & -1 & 2 & \cdots & 0 & 0 \\ \vdots & \vdots & \vdots & \ddots & \vdots & \vdots \\ 0 & 0 & 0 & \cdots & 2 & -1 \\ -1 & 0 & 0 & \cdots & -1 & 2 \end{pmatrix} \qquad P > 2. \tag{19b}$$

Let κ_j be the eigenvalues of a_P, and $\boldsymbol{u}_j$ the corresponding normalized eigenvectors. The values of κ_j depend on P (see appendix B and table 1). Where no confusion can arise, in what follows we do not explicitly denote all the dependences of κ_j, $\boldsymbol{u}_j$, and many other quantities to avoid complicated notation.

With this choice of $\boldsymbol{u}_j$, let us define new coordinates ξ_j again using the transformation (14). It is obvious from equations (19) that for arbitrary $P \geqslant 2$ one of

Table 1. List of the doubly degenerate eigenvalues of the matrix a_P for small values of P.

P	κ_j
3	3
4	2
5	$(5 \mp \sqrt{5})/2$
6	1, 3
7	$[7 - 2\sqrt{7}\cos(\varphi/3)]/3$, $[7 + \sqrt{7}\cos(\varphi/3)]/3 \mp \sqrt{(7/3)}\sin(\varphi/3)$[a]
8	$2, 2 \mp \sqrt{2}$
9	$3, 2[1 + \cos(\pi/9)], 2 - \cos(\pi/9) \mp \sqrt{3}\sin(\pi/9)$
10	$(3 \mp \sqrt{5})/2, (5 \mp \sqrt{5})/2$
12	$2, 1, 3, 2 \mp \sqrt{3}$
14	$[7 - 2\sqrt{7}\cos(\varphi/3)]/3$, $[7 + \sqrt{7}\cos(\varphi/3)]/3 \mp \sqrt{(7/3)}\sin(\varphi/3)$, $[5 + 2\sqrt{7}\cos(\varphi/3)]/3$, $[5 - \sqrt{7}\cos(\varphi/3)]/3 \mp \sqrt{(7/3)}\sin(\varphi/3)$[a]
15	$3, (5 \mp \sqrt{5})/2, [7 - \sqrt{5} \mp \sqrt{6(5 - \sqrt{5})}]/4, [7 + \sqrt{5} \mp \sqrt{6(5 + \sqrt{5})}]/4$
16	$2, 2 \mp \sqrt{2}, 2 \mp \sqrt{2 - \sqrt{2}}, 2 \mp \sqrt{2 + \sqrt{2}}$
18	$1, 3, 2[1 \mp \cos(\pi/9)], 2 \mp \cos(\pi/9) + \sqrt{3}\sin(\pi/9), 2 \mp \cos(\pi/9) - \sqrt{3}\sin(\pi/9)$
20	$2, (3 \mp \sqrt{5})/2, (5 \mp \sqrt{5})/2, 2 \mp \sqrt{(5 - \sqrt{5})/2}, 2 \mp \sqrt{(5 + \sqrt{5})/2}$

[a] Here $\cos\varphi = 1/(2\sqrt{7})$ and $0 < \varphi < \pi/2$.

the eigenvalues of a_P is always zero, let us say $\kappa_1 = 0$, and the corresponding eigenvector is given by equation (13). Thus we may write

$$x_i = \frac{\xi_1}{\sqrt{P}} + \sum_{j=2}^{P} \xi_j u_{ji}. \tag{20}$$

Because a_P is a real symmetric matrix, $\boldsymbol{u}_j$ constitute an orthonormal basis:

$$\sum_{i=1}^{P} u_{ji} u_{ki} = \delta_{jk}. \tag{21}$$

As a result of this orthonormality, the last term in equation (20) represents a component of a vector perpendicular to the main diagonal. Using equations (20) and (21), one gets the normal form

$$\alpha_P = \frac{C\pi}{\beta} \sum_{j=2}^{P} \kappa_j \xi_j^2. \tag{22}$$

Substituting this into equation (1) and switching to the ξ coordinates gives

$$Q_P = C^{(P/2)} \int_{\sqrt{P}x_{\min}}^{\sqrt{P}x_{\max}} \mathrm{d}\xi_1 \int_{-\infty}^{+\infty} \mathrm{d}\xi_2 \cdots \int_{-\infty}^{+\infty} \mathrm{d}\xi_P \exp\left[- C\pi \sum_{j=2}^{P} \kappa_j \xi_j^2 - \beta\lambda_P \right]. \tag{23}$$

Here we have already made an approximation by extending the integration limits in the directions $\xi_2, \ldots, \xi_P$ (perpendicular to the main diagonal) to infinity. When $x_{\min} = -\infty$ and $x_{\max} = +\infty$ (such as for the harmonic oscillator), this is no approximation at all. For the truncated 9–3 potential, we have verified in the previous section that this extension of integration limits does not change the results significantly for high temperatures.

For high temperatures, we know that the integrand in equation (23) is significantly different from zero only for $\xi_j \approx 0$; $j \geqslant 2$. Here one can expand $V(x_t)$ present in λ_P into a Taylor series at $x = \xi_1/\sqrt{P}$ (the common centre of mass of all particles) and truncate the

expansion after the term of degree 2 if $V''(x) > 0$, or otherwise also neglect the second-degree term. In this way, using equation (20) and (21),

$$\begin{aligned}\lambda_P &= \frac{1}{P}\sum_{t=1}^{P} V\left(x + \sum_{j=2}^{P} \xi_j\, u_{jt}\right) \\ &\approx \frac{1}{P}\sum_{t=1}^{P}\left[V(x) + V'(x)\sum_{j=2}^{P}\xi_j u_{jt} + \tfrac{1}{2}\max(V''(x),0)\left(\sum_{j=2}^{P}\xi_j\, u_{jt}\right)^2\right] \\ &= V(x) + \frac{1}{2P}\max(V''(x),0)\sum_{j=2}^{P}\xi_j^2 \qquad (24)\end{aligned}$$

where $x = \xi_1/\sqrt{P}$. Substituting this truncated Taylor series into equation (23) gives the desired high-temperature approximation for Q_P:

$$Q_P^{(\mathrm{hT})} = C^{P/2}\sqrt{P}\int_{x_{\min}}^{x_{\max}} \mathrm{d}x\, \mathrm{e}^{-\beta V(x)} \prod_{j=2}^{P}\int_{-\infty}^{+\infty} \mathrm{e}^{-\gamma_j(x)\xi_j^2}\,\mathrm{d}\xi_j$$

where $\gamma_j(x) = C\pi\kappa_j + (\beta/2P)\max(V''(x),0)$. The integrals over ξ_j can now be evaluated analytically, and we get

$$Q_P^{(\mathrm{hT})} = \sqrt{P}C^{P/2}q_P \qquad (25a)$$

$$q_P = \int_{x_{\min}}^{x_{\max}} B(x)\mathrm{e}^{-\beta V(x)}\,\mathrm{d}x \qquad B(x) = \prod_{j=2}^{P}\sqrt{\frac{\pi}{\gamma_j(x)}}. \qquad (25b)$$

Using the same approximations for $\langle\alpha_P\rangle$ and $\langle\lambda_P\rangle$ gives

$$\langle\alpha_P\rangle^{(\mathrm{hT})} = \frac{\overline{\alpha_P}}{q_P} \qquad (26a)$$

$$\overline{\alpha_P} = \frac{C\pi}{2\beta}\int_{x_{\min}}^{x_{\max}}\left[\sum_{j=2}^{P}\frac{\kappa_j}{\gamma_j(x)}\right]B(x)\mathrm{e}^{-\beta V(x)}\,\mathrm{d}x \qquad (26b)$$

and

$$\langle\lambda_P\rangle^{(\mathrm{hT})} = \frac{\overline{\lambda_P}}{q_P} \qquad (27a)$$

$$\overline{\lambda_P} = \int_{x_{\min}}^{x_{\max}}\left[V(x) + \frac{1}{4P}\max(V''(x),0)\sum_{j=2}^{P}\frac{1}{\gamma_j(x)}\right]B(x)\mathrm{e}^{-\beta V(x)}\,\mathrm{d}x. \qquad (27b)$$

When deriving these formule, approximation (24) was used for all occurrences of λ_P. Note that one could further improve equation (27*b*) by including an arbitrary number of terms in the Taylor series of λ_P when λ_P occurs as the prefactor of $\mathrm{e}^{-\beta U_P}$(in the role of the $A_P(x_1,\ldots,x_P)$ term of equation (12)) while retaining at most the term of degree 2 in $\mathrm{e}^{-\beta U_P}$. This would lead to the appearance of additional terms inside the square brackets of equation (27*b*) proportional to even-order derivatives of $V(x)$, and the rest of the integrand would remain unchanged. However, these additional terms would also be dependent on the components of $\boldsymbol{u}_j$, which would complicate the computation considerably. For example, the next term inside the square brackets would be $(1/32P)V^{(4)}(x)T_4(x)$, where

$$T_4(x) = \sum_{j=2}^{P}\frac{1}{\gamma_j(x)^2}\sum_{i=1}^{P}u_{ji}^4 + 2\sum_{j=2}^{P-1}\sum_{k=j+1}^{P}\frac{1}{\gamma_j(x)\gamma_k(x)}\sum_{i=1}^{P}u_{ji}^2u_{ki}^2. \qquad (28)$$

Proceeding in the same way for the virial estimator of equation (11), we get

$$\langle \epsilon_P^{\mathrm{vir0}} \rangle^{(\mathrm{hT})} = \frac{\overline{\epsilon_P^{\mathrm{vir0}}}}{q_P} \tag{29a}$$

$$\overline{\epsilon_P^{\mathrm{vir0}}} = \int_{x_{\min}}^{x_{\max}} \left[f(x) + \frac{1}{4P} f''(x) \sum_{j=2}^{P} \frac{1}{\gamma_j(x)} + \frac{1}{32P} f^{(4)}(x) T_4(x) + \cdots \right] B(x) \mathrm{e}^{-\beta V(x)} \, \mathrm{d}x \tag{29b}$$

where

$$f^{(2k)}(x) = (k+1)V^{(2k)}(x) + \tfrac{1}{2}(x-L)V^{(2k+1)}(x) \qquad k \geqslant 0.$$

Dropping the $-L$ term in this formula gives the expression for $\langle \epsilon_P^{\mathrm{vir}} \rangle^{(\mathrm{hT})}$ (cf equation (6)) suitable for $x_{\min} = -\infty$ and $x_{\max} = +\infty$. The HTPIQMC results presented below have been obtained using only the harmonic approximation (27*b*), neglecting all the terms proportional to $f^{(4)}(x)$ and higher derivatives of $f(x)$ in equation (29*b*).

Note that equation (25*b*), (26*b*), (27*b*), and (29*b*) have the form of the classical averages of position-dependent functions $B(x)$, $(C\pi/2\beta)\sum_{j=2}^{P}[\kappa_j/\gamma_j(x)]B(x)$, etc, over a classical canonical ensemble corresponding to the potential $V(x)$. In principle, one can use the classical MC simulation to calculate these averages. In the present case, it is of course much simpler to carry out the remaining one-dimensional integration in equations (25*b*), (26*b*), (27*b*), and (29*b*) numerically (we have used the Romberg interpolation scheme for this purpose). However, a generalization of this approximation to the case of many quantum particles could naturally lead to such an essentially classical MC simulation involving certain quantum corrections while retaining a number of degrees of freedom comparable to the classical case, which is a major gain in efficiency.

A similar approximation can be derived for the particle density $\rho_P(x)$ of equation (3). As we observed in the previous section, $\mathrm{e}^{-\beta U_P}$ for a given $x \equiv x_1$ is significantly different from zero only for $x_2 \approx x_3 \approx \cdots \approx x_P \approx x$. It is thus possible to truncate the Taylor series for U_P, keeping only the terms of at most degree 2 or less,

$$y_i = x_{i+1} - x \qquad i = 1, \ldots, P-1$$

to get

$$U_P \approx C\left[y_1^2 + \sum_{j=1}^{P-2} (y_i - y_{i+1})^2 + y_{P-1}^2 \right] + V(x) + \frac{1}{P} \sum_{j=1}^{P-1} [V'(x) y_i + \tfrac{1}{2} \max(0, V''(x)) y_i^2]$$

(here the terms originating from α_P are exact). This can be rewritten as

$$U_P \approx V(x) + \boldsymbol{b} \cdot \boldsymbol{y} + C\, \boldsymbol{y} \cdot \tilde{a}_{P-1} \cdot \boldsymbol{y} \tag{30}$$

where all the elements of $\boldsymbol{b}$ are identical, $b_i = (1/P)V'(x)$, and $\tilde{a}_{P-1}$ is a tridiagonal matrix of the order $P-1$ with the following non-zero elements:

$$\begin{aligned} &(\tilde{a}_{P-1})_{ii} = 2 + \delta \qquad \delta = (1/2PC)\max(0, V''(x)) \\ &(\tilde{a}_{P-1})_{ij} = -1 \qquad \text{if } |i-j| = 1. \end{aligned} \tag{31}$$

Substituting equation (30) into equation (3) and extending the integration limits to $\pm\infty$ in all integrals (justified for high temperatures) gives

$$\rho_P^{(\mathrm{hT})}(x) = C^{P/2} \mathrm{e}^{-\beta V(x)} \int_{-\infty}^{+\infty} \mathrm{d}y_1 \cdots \int_{-\infty}^{+\infty} \mathrm{d}y_P \exp(-\beta C \boldsymbol{y} \cdot \tilde{a}_{P-1} \cdot \boldsymbol{y} - \beta \boldsymbol{b} \cdot \boldsymbol{y}).$$

Again using a transformation of type (14), where $\boldsymbol{u}_i$ are now eigenvectors of the matrix (31), this can be evaluated analytically [22] to give

$$\rho_P^{(\mathrm{hT})}(x) = \left(\frac{C}{\det(\tilde{a}_{P-1})}\right)^{\frac{1}{2}} \left(\frac{\pi}{\beta}\right)^{(P-1)/2} \mathrm{e}^{-\beta V(x)} \exp\left[\frac{\beta}{4C}\boldsymbol{b}\cdot\tilde{a}_{P-1}^{-1}\cdot\boldsymbol{b}\right]. \quad (32)$$

The determinant $\det(\tilde{a}_{P-1})$ is given by equation (C1) and (C2) of appendix C. The matrix product in the argument of the last exponential is

$$\boldsymbol{b}\cdot\tilde{a}_{P-1}^{-1}\cdot\boldsymbol{b} = \left[\frac{1}{PV'(x)}\right]^2 S_{P-1}$$

where $S_n = \sum_{i=1}^{n}\sum_{j=1}^{n}(\tilde{a}_n^{-1})_{ij}$. The sum S_n of all elements of the inverse matrix $\tilde{a}_n^{-1}$ is given by equation (C3) of appendix C.

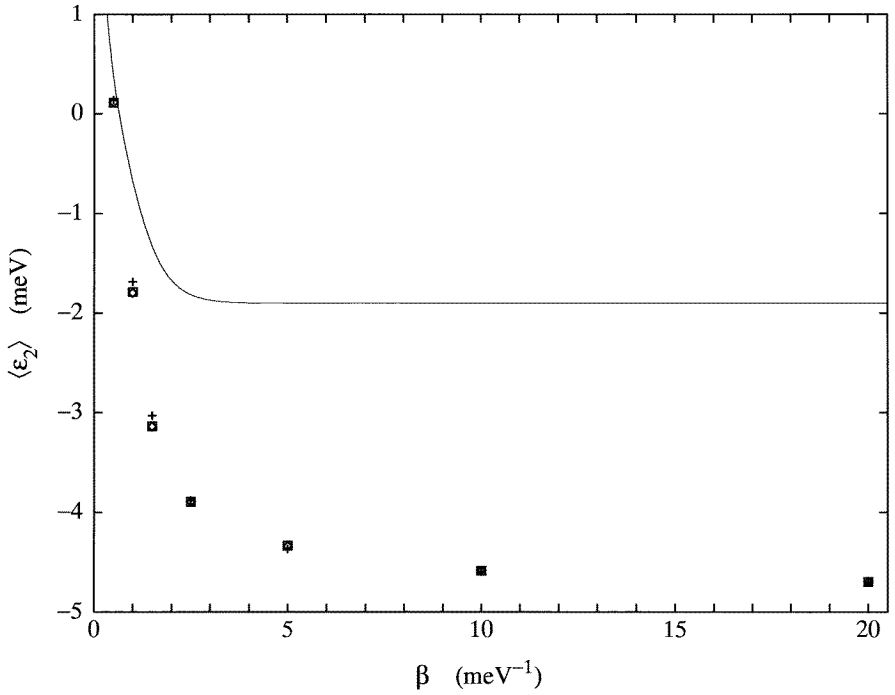

Figure 8. Comparison of the HTPIQMC results of section 5 for the 9–3 potential with the exact PIQMC results, from direct Halton integration. $P = 2$. Boxes (□): HTPIQMC values of $\langle\epsilon_2\rangle$ obtained using equations (25)–(27). Diamonds (◇): HTPIQMC values of $\langle\epsilon_2\rangle$ obtained using the modified formule corresponding to the finite integration limits in the ξ_2 direction (such that the resulting two-dimensional integral is over the square $0 < x_{1,2} < L/\sigma$). Crosses (+): the values of $\langle\epsilon_2\rangle$ obtained by Halton integration. Same potential as in figure 1, $L = 40$ Å. The full curve represents the exact value of $\langle E\rangle$ of equation (A4).

For $P = 2$, it is easy to find the exact integration limits for ξ_2 in equation (23). In figure 8 results obtained with such exact integration limits are compared with the standard HTPIQMC results corresponding to $\int_{-\infty}^{\infty} \mathrm{d}\xi_2$. One can see, that they are practically identical. This again supports the assumption that the extension of integration limits to infinity does not introduce any significant error.

What is somewhat surprising in figure 8 is the fact that for arbitrary β, the HTPIQMC results for $P = 2$ are very close to the exact PIQMC results for $P = 2$, which can be

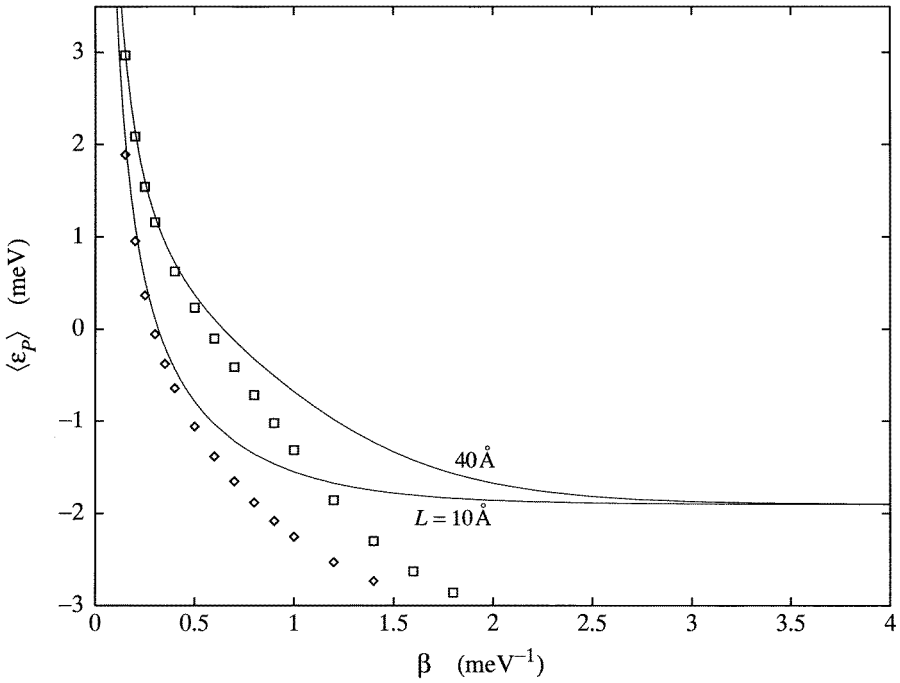

Figure 9. The HTPIQMC values of $\langle \epsilon_P \rangle$ obtained in the limit $P \to \infty$ ($P = 256$) for the same 9–3 potential as in figure 1. Diamonds (◇): $L = 10$ Å; boxes (□): $L = 40$ Å. The full curves labelled by L represent the exact values of $\langle E \rangle$ of equation (A4).

obtained very easily by the direct Halton integration of the previous section (much faster than PIQMC simulation). Of course, except for the smallest values of β, the $P = 2$ results are far from the exact ($P = \infty$) results. As P increases, the close agreement of the HTPIQMC and the exact PIQMC results is maintained only for small values of β. This can be seen in figure 9 where the HTPIQMC results are compared with the exact values of $\langle E \rangle$. In the $P \to \infty$ limit, the exact PIQMC results must be identical with the exact $\langle E \rangle$ values. Thus for the 9–3 potential, the HTPIQMC method is indeed a high-temperature approximation. The HTPIQMC value for $\langle \epsilon_P^{\mathrm{vir0}} \rangle$ is consistently below that for $\langle \epsilon_P \rangle$ even for the smallest β.

In figure 10 we present the HTPIQMC density obtained using equation (32). One can see that it agrees with the exact density quite well everywhere, except near the peak. Similar plots were obtained for a large range of β, with the excess HTPIQMC density at the peak increasing with β.

Equations (25) can also be written in the form of a classical expression,

$$Q_P^{(\mathrm{hT})} = \sqrt{\frac{m}{2\pi\hbar^2\beta}} \int_{x_{\min}}^{x_{\max}} \mathrm{e}^{-\beta V_{\mathrm{eff}}(x)}\, \mathrm{d}x$$

where

$$V_{\mathrm{eff}}(x) = V(x) - \frac{1}{\beta} \ln \left[P C^{(P-1)/2} B(x) \right].$$

Note that the form of our effective potential $V_{\mathrm{eff}}(x)$ is very different from the Gaussian transform form of the Feynman–Hibbs effective potential, see for example equations (3.81) and (3.90) of [3].

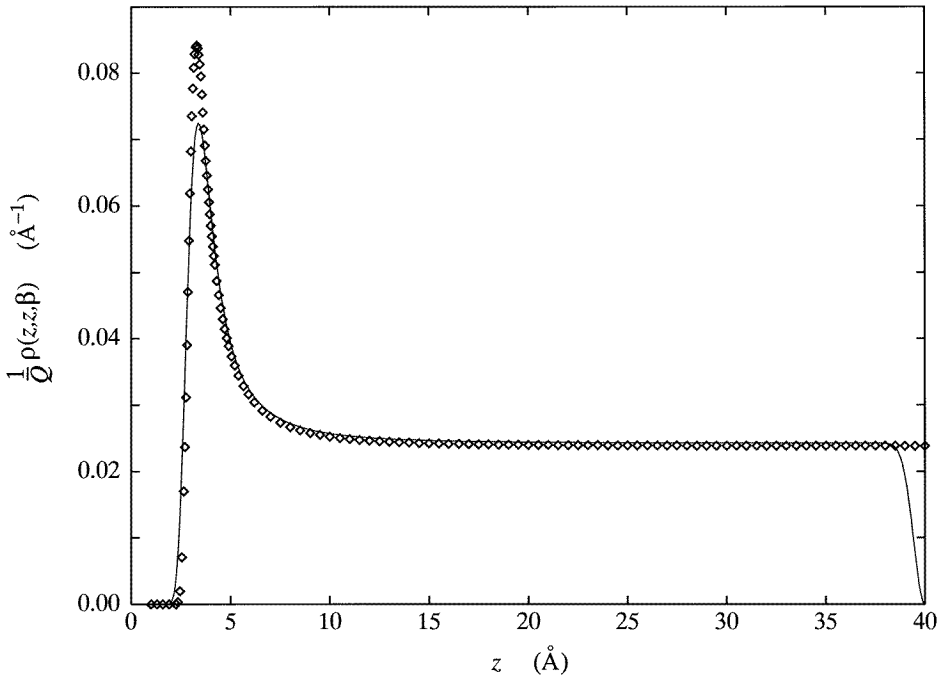

Figure 10. Comparison of the exact normalized particle density (full curve) with the $P \to \infty$ HTPIQMC results (◇) for $\beta = 0.3$ meV^{-1} for the same 9–3 potential as in figure 1 with $L = 40$ Å.

Let us now compare our HTPIQMC method with the two previous approximations of comparable complexity—with the above-mentioned Feynman–Hibbs effective potential, and with the simplest form of the partial averaging of the Fourier PIQMC of Doll *et al* [10] corresponding to $k_{\max} = 0$ in their formule. Whereas our $P \to \infty$ HTPIQMC method gives exact results for the harmonic oscillator potential, the two previous methods do not. Furthermore, they cannot be applied at all to the 9–3 potential because of its behaviour at $x = 0_+$, whereas the HTPIQMC method gives, for small β, satisfactory results even for this difficult case. Finally, let us compare the three methods for the quartic oscillator with $V(x) = \frac{1}{2}x^4 (m = \hbar = 1)$. For this case, the Feynman–Hibbs effective potential method [3] gives

$$Q \approx \sqrt{\frac{1}{2\pi\beta}} \int_{-\infty}^{\infty} \exp\left[-\frac{\beta}{2}\left(y^4 + \frac{\beta}{2}y^2 + \frac{\beta^2}{48}\right)\right] \mathrm{d}y$$

and the $k_{\max} = 0$ form of the partial averaging approach [10]

$$Q \approx \sqrt{\frac{1}{2\pi\beta}} \int_{-\infty}^{\infty} \exp\left[-\frac{\beta}{2}\left(x^4 + \beta x^2 + \frac{\beta^2}{10}\right)\right] \mathrm{d}x.$$

Using these two approximations for Q in equation (4) gives the approximations for $\langle E \rangle$ that are presented in figure 11 together with the HTPIQMC $P \to \infty$ results. One can see that for all β the HTPIQMC results are much closer to the exact values of $\langle E \rangle$ (obtained again using the procedure of [27]) than the results of the other two approximations. Whereas these two methods always give an upper bound for the (free) energy, from the way our

high-temperature approximation for λ_p was derived, it seems that it could, most of the time, give a *lower bound* of the energy.

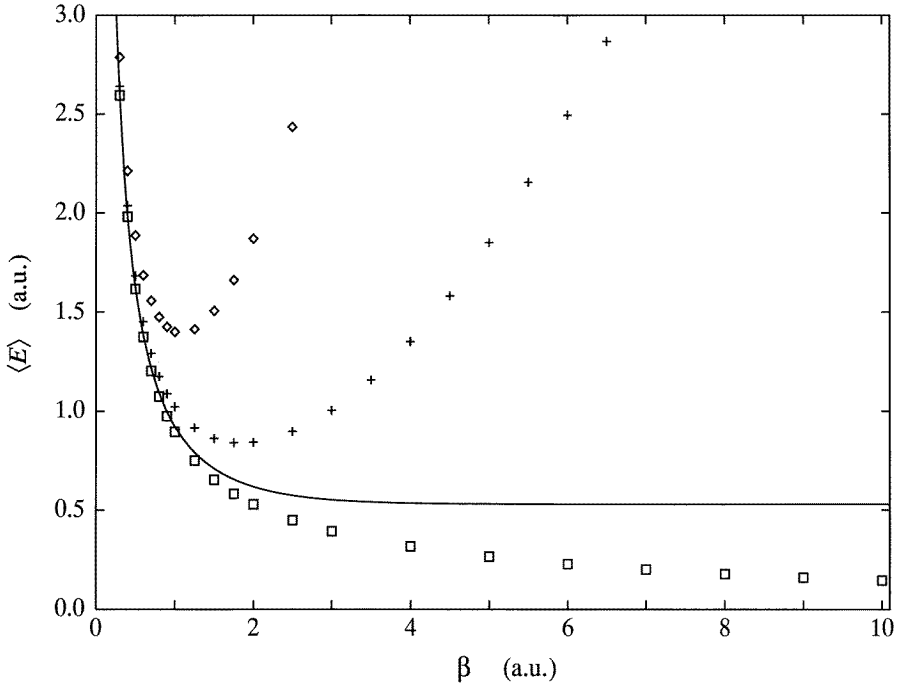

Figure 11. The HTPIQMC $P \to \infty$ values (□) of $\langle \epsilon_P \rangle$ for the quartic oscillator potential $V(x) = \frac{1}{2}x^4 (m = \hbar = 1)$. For comparison, the results obtained with two other approximations of comparable complexity—with the Feynmann–Hibbs effective potential method (+) and the simplest form of the partial averaging approach (◊)—are also shown. The full curve represents the exact value of $\langle E \rangle$.

Unlike in the case of the 9–3 potential, for the quartic oscillator the HTPIQMC procedure gives practically identical estimates for $\langle \epsilon_P^{\text{vir}} \rangle$ and $\langle \epsilon_P \rangle$. The HTPIQMC density is again larger near the peak (at $x = 0$) than the exact density.

The CPU time required for an HTPIQMC calculation using $P \leqslant 256$ is orders of magnitude smaller than that for full PIQMC simulations or from direct Halton integration of comparable accuracy. For $P = 2^n$ with $n > 8$, one usually encounters overflows when calculating the integrands of equation (25*b*) to (29*b*); however, the convergence (as $P \to \infty$) is usually achieved well before $P = 256$. For $P = 2^n$ we use equation (B9).

6. Calculation of the configurational partition function Q_P

In this section, we discuss the possibility of obtaining the β dependence of Q_P in a single PIQMC run. Note that in section 4 and 5 we were able to calculate directly the absolute values of the partition function Q_P. Especially for smaller β, both methods are quite reliable and give identical results. On the other hand, a direct calculation of the values of a partition function in the usual MC simulation, for example, using the method of Salzburg *et al* [23] (i.e. using $A_P(x_i) = \mathrm{e}^{+\beta U_P}$ in equation (12)), is known to be flawed (e.g. [24]). However, a suitable choice of $A_P(x_i)$ can yield the β dependence of the partition function in a certain

range of β in a *single* PIQMC run. Substituting

$$A_P(x_i) = \exp[\beta U_P(\beta) - \tilde{\beta} U_P(\tilde{\beta})] \tag{33}$$

into equation (12) gives

$$\langle \exp[\beta U_P(\beta) - \tilde{\beta} U_P(\tilde{\beta})] \rangle_\beta = \left[\frac{C(\beta)}{C(\tilde{\beta})}\right]^{P/2} \frac{Q_P(\tilde{\beta})}{Q_P(\beta)}. \tag{34}$$

Here we denote explicitly the dependence of all the quantities on the inverse temperature β, and $\langle\ \rangle_\beta$ means that the canonical ensemble average is calculated at β.

In the case studied here, $U_P(\beta) = \alpha_P(\beta) + \lambda_P$, where $\alpha_P(\beta) = \overline{\alpha}_P/\beta^2$, cf equation (2), where $\overline{\alpha}_P$ and λ_P do not depend on β. Substituting this expression into equation (34) gives

$$Q_P(\tilde{\beta}) = Q_P(\beta) \left(\frac{\beta}{\tilde{\beta}}\right)^{P/2} \left\langle \exp\left\{(\beta - \tilde{\beta})\left[-\frac{\beta}{\tilde{\beta}}\alpha_P(\beta) + \lambda_P\right]\right\}\right\rangle_\beta . \tag{35}$$

Choosing $0 < \tilde{\beta} \ll \beta$ here gives a very small value of the exponential in most of the configurational space (except in the vicinity of the main diagonal). This would make it possible to obtain the ratio $Q_P(\tilde{\beta})/Q_P(\beta)$ for an arbitrary number of values of $\tilde{\beta}$, i.e. the $\tilde{\beta}$ dependence of $Q_P(\tilde{\beta})$ in a single PIQMC simulation performed at a larger value of β. A different method to achieve the same goal has recently been proposed by Lyubartsev *et al* [25] who use multi-temperature expansion of the canonical ensemble. Here all the averaging is done at a single temperature β, using a series of estimators of equation (33) for the other temperatures.

We have tested this approach for $P = 2$ where the exact values of $Q_2(\beta)$ (which are of course not identical with $Q_\infty(\beta)$ for large β) can be quickly calculated by the HTPIQMC method (cf figure 8). The results for $\beta = 0.5$ meV^{-1} are presented in figure 12. For $\tilde{\beta} < \beta$, excellent agreement with the exact values of $Q_P(\tilde{\beta})/Q_P(\beta)$ has been obtained. As expected, $\tilde{\beta} > \beta$ gives consistently smaller values of $Q_P(\tilde{\beta})/Q_P(\beta)$ because the first term of the exponent in equation (35) is positive and very large far from the main diagonal where the sampling is expected to be poor. Further testing is needed for larger values of P.

7. Summary

The main achievement of this paper is the introduction of a high-temperature approximation for the PIQMC method. This approximate method requires a negligible fraction of the CPU time needed for standard PIQMC simulations, and has the potential for further improvement by including higher-order terms in the local expansion of the potential. It gives exact results for the harmonic oscillator potential, and it can be expected to be superior to previous approximations of comparable complexity for a large class of potentials dealing with molecular oscillations. Generalization of this approximate method to more complex systems of interacting quantum particles requires further study.

A method for obtaining the temperature dependence of the configurational partition functions in a single PIQMC run was proposed.

We have also found that even the corrected virial total-energy estimator that takes into account the finiteness of the system is not very useful for the truncated 9–3 potential of appendix A. For the values of P already large enough to give the $P \to \infty$ limit satisfactorily, its convergence with the number of MC cycles is much worse than that of the direct total-energy estimator.

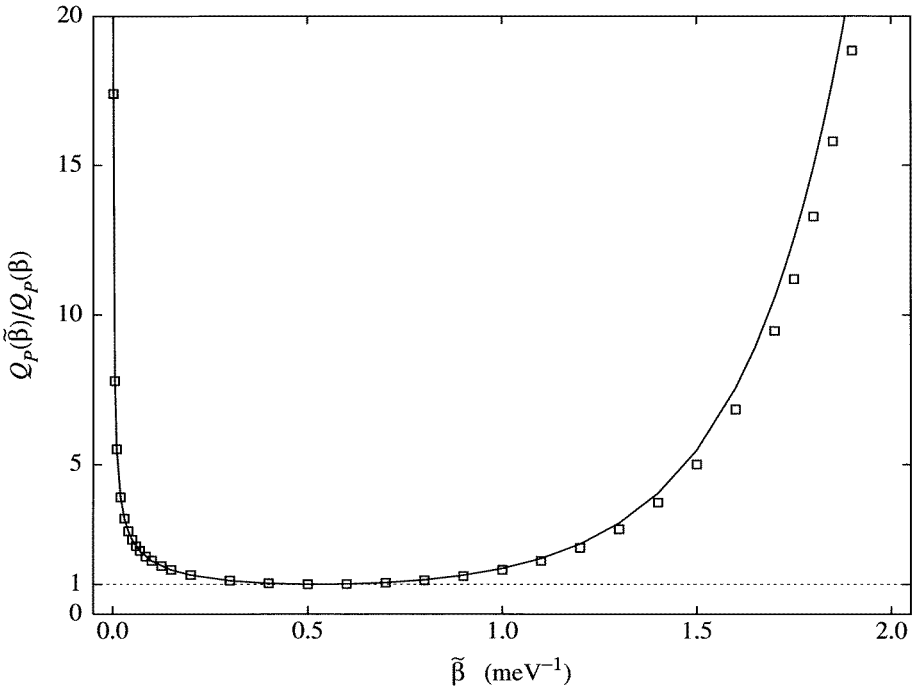

Figure 12. Boxes (□) represent the PIQMC ratio $Q_P(\tilde{\beta})/Q_P(\beta)$ for $P = 2$ and $\beta = 0.5\,\mathrm{meV}^{-1}$, obtained for the 9–3 potential after 5×10^7 MC cycles using equation (35). The full curve represents the exact values (obtained by the HTPIQMC method, cf figure 8). Other parameters are the same as in figure 1.

Acknowledgment

This research was supported by a grant from the Natural Sciences and Engineering Research Council of Canada.

Appendix A. 9–3 potential

A solid occupying the left ($z < 0$) half of the space is approximated by a continuum of inert atoms that interact with an adatom positioned somewhere in the $z > 0$ half of the space via a Lennard–Jones potential. Then the resulting potential experienced by the adatom is [26]

$$V(z) = \frac{1}{2}V_m\left[\left(\frac{z_0}{z}\right)^9 - 3\left(\frac{z_0}{z}\right)^3\right] \qquad z > 0. \tag{A1}$$

Here $V_m > 0$ and $z_0 > 0$. This 9–3 potential has a minimum equal to $-V_m$ at $z = z_0$. Because a MC simulation cannot sample an infinite region in finite time, we have to add an infinitely high wall to $V(z)$ at $z = L > 0$ (assume $V(z) = \infty$ for $z > L$). Let E_n be the eigenvalues of the truncated Hamiltonian,

$$H = -\frac{\hbar^2}{2m}\frac{\mathrm{d}^2}{\mathrm{d}z^2} + V(z) \qquad 0 < z < L \tag{A2}$$

where $V(z)$ is given by equation (A1). To find E_n, it is convenient to introduce atomic-like units by scaling $z = \sigma x$ and $H = (\overline{h}^2/m\sigma^2\mathcal{H})$. Then

$$\mathcal{H} = -\frac{1}{2}\frac{\mathrm{d}^2}{\mathrm{d}x^2} + \frac{c_1}{x^9} - \frac{c_2}{x^3} \qquad 0 < x < \frac{L}{\sigma} \tag{A3}$$

where $c_1 = \frac{1}{2}(mV_m z_0^9/\sigma^7\overline{h}^2)$ and $c_2 = \frac{3}{2}(mV_m z_0^3/\sigma\overline{h}^2)$. Using $\sigma^2 = \frac{1}{3}\overline{h}z_0/(3mV_m)^{1/2}$ will result in the quadratic coefficient in the expansion of the potential about its minimum being equal to $\frac{1}{2}$. The best way to find the spectrum of the Hamiltonian (A3) seems to be the diagonalization in the discretized coordinate representation [27]. The results obtained in this way are referred to as 'exact' quantum-mechanical results. The values of $\langle E\rangle$,

$$\langle E\rangle = \sum_n E_n \mathrm{e}^{-\beta E_n} \Big/ \sum_n \mathrm{e}^{-\beta E_n} \tag{A4}$$

obtained in this way serve as reference data for the comparison with the QPIMC simulations.

Appendix B. Eigenvalues of the matrix a_P

Let κ be an eigenvalue of the matrix a_P of equation (19*b*) and $\boldsymbol{u}$ the corresponding eigenvector. Denote $K = 2 - \kappa$. Applying the first $P-1$ rows of a_P to $\boldsymbol{u}$ gives

$$u_j = d_j u_1 - d_{j-1} u_P \qquad j = 1, \ldots, P \tag{B1}$$

where

$$d_0 = 0 \qquad d_1 = 1 \qquad d_{j+1} = K d_j - d_{j-1}. \tag{B2}$$

Applying the last row of a_P to $\boldsymbol{u}$ gives

$$u_1 = K u_P - u_{P-1} = d_{P+1} u_1 - d_P u_P.$$

This equation and equation (B1) for $j = P$ constitute a system of two equations for the unknown u_1 and u_P. This system has a non-trivial solution if its determinant is zero. This requirement results in the characteristic equation of the matrix a_P in the form $\chi_P = 0$, where the characteristic polynomial is

$$\chi_P = d_{P+1} - d_{P-1} - 2. \tag{B3}$$

Here we have used the fact that d_j, as introduced by equation (B1), is identical to the Chebyshev polynomial of the first kind $S_{j-1}(K)$ (see e.g. equations (A2) and (A3) of [28]). One can also write $\chi_P = 2\,T_P(K/2) - 2$, where $T_j(x)$ is another, the most often used, Chebyshev polynomial of the first kind. Again using equation (A3) of [28], we can rewrite equation (B3) as

$$\chi_{2k-1} = (K-2)(d_k + d_{k-1})^2 \qquad \chi_{2k} = (K^2-4)d_k^2. \tag{B4}$$

This gives the correct eigenvalues ($\kappa_1 = 0$, $\kappa_2 = 4$) also for a_2 of equation (19*a*). Equation (B4) reflects the fact that one eigenvalue is always $\kappa = 0$ ($K = 2$) for all P. Furthermore, for all even P another eigenvalue is always $\kappa = 4$ ($K = -2$). All other eigenvalues are doubly degenerate, being the roots of $d_k = 0$ for $P = 2k$ and $d_k + d_{k-1} = 0$ for $P = 2k-1$. Note that d_{2l} is always divisible by K. Thus for $P = 4l$ there is always a doubly degenerate eigenvalue $\kappa = 2$ ($K = 0$).

One can evidently write d_k as follows:

$$\begin{aligned} |K| \leqslant 2: &\qquad K = 2\cos\psi \qquad d_k = \frac{\sin k\psi}{\sin\psi} \\ |K| \geqslant 2: &\qquad K = 2\cosh\Psi \qquad d_k = \frac{\sinh k\Psi}{\sinh\Psi}. \end{aligned} \tag{B5}$$

Substituting these explicit expressions into equation (B4), one can see that all the roots of $\chi_P = 0$ are contained in the interval $|K| \leqslant 2$ for all P. Obviously, all the doubly degenerate roots can be written as

$$K_j^{(P)} = 2\cos\left(j\frac{2\pi}{P}\right) \qquad k = 1, 2, \ldots, \lfloor (P-1)/2 \rfloor$$

where $\lfloor x \rfloor$ denotes the integer part of x. Thus all the doubly degenerate eigenvalues of a_P are

$$\kappa_j^{(P)} = 2\left[1 - \cos\left(j\frac{2\pi}{P}\right)\right] \qquad k = 1, 2, \ldots, \lfloor (P-1)/2 \rfloor. \tag{B6}$$

If $P = P_1 P_2$, then $\kappa_{jP_1}^{(P)} = \kappa_j^{(P_2)}$. That means that a_P inherits all the eigenvalues from all $a_{P'}$ such that P' is a factor of P. For all $P = 2k$, one can further write

$$\begin{aligned} j < k/2: &\qquad \kappa_j^{(2k)} = 2 - \sqrt{\kappa_{k-2j}^{(2k)}} \\ j > k/2: &\qquad \kappa_j^{(2k)} = 2 + \sqrt{\kappa_{2j-k}^{(2k)}}. \end{aligned} \tag{B7}$$

In this way one can express every doubly degenerate eigenvalue in terms of another doubly degenerate eigenvalue. The exception is $\kappa_l^{(4l)} = 2$, which can be written formally in the same form but in terms of the non-degenerate eigenvalue $\kappa = 0$: $2 = 2 \pm \sqrt{0}$. A group of the eigenvalues can be connected through equation (B7) in such a way that they constitute a closed loop. More than one closed loop can exist for a given P. For example, for $P = 14$, there is one loop

$$\kappa_1 = 2 - \sqrt{\kappa_5} \qquad \kappa_5 = 2 + \sqrt{\kappa_3} \qquad \kappa_3 = 2 - \sqrt{\kappa_1}$$

and for the rest we have

$$\kappa_4 = 2 + \sqrt{\kappa_1} \qquad \kappa_6 = 2 + \sqrt{\kappa_5} \qquad \kappa_2 = 2 - \sqrt{\kappa_3}.$$

For $P = 210$, there are eight loops. The number of loops and their lengths seem to be related to the prime decomposition of P.

No such relations exist for odd P.

A special case is $P = 2^l$ when there are no loops, and all the relations (B7) constitute a single tree with its root at $\kappa = 2$. To show this, let us renumber the eigenvalues in a different way than as given above. Let us define

$$\psi_1 = \frac{\pi}{2} \qquad \psi_{2j} = \frac{\pi - \psi_j}{2} \qquad \psi_{2j+1} = \frac{\pi + \psi_j}{2}.$$

Then for $\kappa_j = 2(1 - \cos\psi_j)$ we have

$$\kappa_1 = 2 \qquad \kappa_{2j} = 2 - \sqrt{\kappa_j} \qquad \kappa_{2j+1} = 2 + \sqrt{\kappa_j} \qquad j = 1, 2, \ldots, 2^{l-2} - 1. \tag{B8}$$

Thus for $P = 2^l$, all the doubly degenerate eigenvalues can be written as

$$\kappa_j = 2 \mp \sqrt{2 \mp \sqrt{2 \mp \cdots \mp \sqrt{2}}} \tag{B9}$$

where there are between 0 and $l - 2$ levels of the square root, and all the sign choices are independent.

For several small values of P, table 1 contains expressions for κ_j alternative to equation (B6). For small β, the values of P of table 1 would be sufficient for most HTPIQMC applications. To see what happens in the limit as $P \to \infty$, the subsequence of $P = 2^l$ can be used with the corresponding κ_j given by equation (B8) or (B9).

Appendix C. Determinant and inverse of the matrix $\tilde{a}_n$

By the minor expansion from the first row, we get the following recursion relation with respect to its order n for the determinant of matrix $\tilde{a}_n$ of equation (31):

$$\det(\tilde{a}_1) = 2 + \delta \qquad \det(\tilde{a}_n) = (2+\delta)\det(\tilde{a}_{n-1}) - \det(\tilde{a}_{n-2}) \qquad n > 1$$

(assuming $\det(\tilde{a}_0) = 1$). Comparing this with equation (B2), we see that

$$\det(\tilde{a}_n) = d_{n+1} \tag{C1}$$

where the argument of the Chebyshev polynomial d_k is now equal to $2+\delta$. Because $\delta \geqslant 0$ by definition, we can use the substitution $2 + \delta = 2\cosh\Psi$, and from equation (B5) we have

$$d_n = \frac{F^{2n} - 1}{F^n \sqrt{\delta(4+\delta)}} \tag{C2}$$

where $F = \mathrm{e}^{\Psi} = 1 + \delta/2 + \frac{1}{2}\sqrt{\delta(4+\delta)}$ (i.e. $\sinh\Psi = \frac{1}{2}\sqrt{\delta(4+\delta)}$).

In the same way, one can express all the minors of $\tilde{a}_n$ in terms of the d_k polynomials of $(2+\delta)$, and get the formula for the elements of the inverse matrix

$$(\tilde{a}_n^{-1})_{ij} = \frac{d_{\min(i,j)} d_{n+1-\max(i,j)}}{d_{n+1}}.$$

Using equation (A3) of [28], one can easily verify that $\tilde{a}_n \tilde{a}_n^{-1} = \mathbf{1}$. What we only need in equation (32) is

$$S_n = \sum_{i=1}^{n}\sum_{j=1}^{n} (\tilde{a}_n^{-1})_{ij} = \frac{1}{d_{n+1}}\left[\sum_{i=1}^{n} d_i d_{n+1-i} + 2\sum_{i=1}^{n-1} d_i \sum_{j=i+1}^{n} d_{n+1-j}\right].$$

Using equation (C2), we obtain after a lengthy manipulation

$$S_n = \frac{1}{\delta}\left[n + 1 - \frac{\sqrt{4+\delta}}{\delta}\frac{F^{n+1} - 1}{F^{n+1} + 1}\right]. \tag{C3}$$

In the limit of $\delta \to 0$, $d_k(2) = 2$ and $S_n = \frac{1}{12}n(n+1)(n+2)$.

References

[1] For example Binder K (ed) 1981 *Monte Carlo Methods in Statistical Physics* (Berlin: Springer)
Heermann D W 1990 *Computer Simulation Methods* (Berlin: Springer)
[2] Feynman R P and Hibbs A R 1965 *Quantum Mechanics and Path Integrals* (New York: McGraw-Hill)
[3] Feynman R P 1972 *Statistical Mechanics* (Reading, MA: Benjamin)
[4] MoritaT 1973 *J. Phys. Soc. Japan* **35** 98
[5] Barker J A 1979 *J. Chem. Phys.* **70** 2914
[6] Herman M F, Bruskin E J and Berne B J 1982 *J. Chem. Phys.* **76** 5150
[7] Thirumalai D, Hall R W and Berne B J 1984 *J. Chem. Phys.* **81** 2523
[8] Berne B J 1986 *J. Stat. Phys.* **43** 911; and other contributions in 1986 *Proc. of the Metropolis Quantum Monte Carlo Conf., J. Stat. Phys.* **43** 729–1244
[9] Doll J D, Freeman D L and Beck T L 1990 *Adv. Chem. Phys.* **78** 61
[10] Doll J D, Coalson R D and Freeman D L 1985 *Phys. Rev. Lett.* **55** 1
Coalson R D, Freeman D L and Doll J D 1986 *J. Chem. Phys.* **85** 4567
[11] Ceperley D M and Pollock E L 1987 *Phys. Rev.* B **36** 8343; 1989 *Phys. Rev.* B **39** 2084
[12] Makri N and Miller W H 1988 *Chem. Phys. Lett.* **151** 1; 1989 *J. Chem. Phys.* **90** 904
Makri N 1991 *Chem. Phys. Lett.* **193** 435
[13] Stump D R 1987 *Phys. Rev.* A **36** 365
[14] Ermakov K V, Butayev B S and Spiridonov V P 1987 *Chem. Phys. Lett.* **138** 153

[15] Zhang P, Levy R M and Friesner R A 1988 *Chem. Phys. Lett.* **144** 236
[16] Mak C H and Andersen H C 1990 *J. Chem. Phys.* **92** 2953
[17] Schweizer K S, Stratt R M, Chandler D and Wolynes P G 1981 *J. Chem. Phys.* **75** 1347
[18] Polanyi J C, Williams R J and O'Shea S F 1991 *J. Chem. Phys.* **94** 978
[19] Berblinger M and Schlier C 1991 *Comput. Phys. Commun.* **66** 157–66
[20] Kolář M and O'Shea S F 1993 *Comput. Math. Appl.* **25** 3
[21] Marsaglia G 1987 *Florida State University Report* FSU-SCRI-87-50
[22] Cramér H 1946 *Mathematical Methods of Statistics* (Princeton, NJ: Princeton University Press) p 118; see also appendix A of [17].
[23] Salzburg Z W, Jacobson J D, Fickett W and Wood W W 1959 *J. Chem. Phys.* **30** 65
Chesnut D A and Salzburg Z W 1963 *J. Chem. Phys.* **38** 2861
[24] Card D N and Valleau J P 1970 *J. Chem. Phys.* **52** 6232
[25] Lyubartsev A P, Martsinovski A A, Shevkunov S V and Vorontsov-Velyaminov P N 1992 *J. Chem. Phys.* **96** 1776
[26] Steele W A 1974 *The Interaction of Gases with Solid Surfaces* (Oxford: Pergamon) p 14
[27] Balint-Kurti G G, Ward C L and Marston C C 1991 *Comput. Phys. Commun.* **67** 285
[28] Kolář M and Ali M K 1990 *Phys. Rev.* A **42** 7112